Multichannel topological waveguide in multilayer Kagome phononic crystal

Yusuke Hata[1‡] and Kenji Tsuruta[1*] ([1]Okayama Univ.)

1. Introduction

Conventional elastic devices, represented by surface acoustic wave (SAW) filter, have 2-dimensional structure. While it is quite stable to fabricate, it has several disadvantages. First, an additional device cannot be mounted directly on top of the structure, which hinders further integration. Second, it is difficult to hold multichannel and multifunctionality in planar structure. On the other hand, 3-dimensional elastic devices can achieve multichannel and multifunctionality with higher integration. In the present study we designed a waveguide perpendicular to substrate with layer-stacked topological phononic crystal.[1)]

Topological phononic crystals (PnCs) are artificial acoustic/elastic structures to realize efficient acoustic-/elastic-wave propagations. Topological insulators have robust boundary states against bend, disorder, and defects.[2)] A lot of study about robust propagation using topological PnCs have been reported.[3-7)] Recently, multilayer waveguides using topological PnCs have been proposed and demonstrated in acoustic system.[8,9)] Multilayer system has not only valley (wave number dependent) degree of freedom (DOF) but also layer DOF, thus layer polarized states appear in that system. Layer polarized states also lead to multichannel features in the waveguides, e.g., layer converter and wave splitter. Furthermore, multilayer is compatible with the development of 3-dimensional integrations. While the study on multilayer topological PnCs in acoustic system is rapidly increasing, the efforts to develop multilayer topological PnCs in elastic system are limited in a specific lattice.[10)]

In this study, we investigate topological boundary modes with Kagome lattice, aiming to develop an efficient multichannel waveguide through the topological band design.

2. Bilayer Kagome phononic crystal

We propose a bilayer Kagome PnC to design multichannel waveguides. Kagome lattice is second order topological insulator;[1,11,12)] the topologically protected states appear in the physical region of two-order lower than the dimension of the system. In the multilayered systems, selective wave transmissions between the layers can be achieved through interconnections vertically implemented in the multichannel waveguides. The schematic drawing of bilayer Kagome lattice is shown in **Fig. 1(a)**. Six sites are bridged by bonds with four different strengths (red, blue, yellow, and green), and upper layer and lower layer are connected with thin (gray dots) bonds. By changing intracell- and intercell-bonds in both upper and lower layer, one can control topology of elastic modes in this structure. We name each state by those strengths. N (neutral) state satisfies $|t_{LI}| = |t_{LO}| = |t_{UI}| = |t_{UO}|$. L_+ (L_-) (layer polarized) state satisfies $|t_{LI}| > |t_{LO}|$ ($|t_{LI}| < |t_{LO}|$) and $|t_{UI}| < |t_{UO}|$ ($|t_{UI}| > |t_{UO}|$). V_+ (V_-) (valley polarized) state satisfies $|t_{LI}| < |t_{LO}|$ ($|t_{LI}| > |t_{LO}|$) and $|t_{UI}| < |t_{UO}|$ ($|t_{UI}| > |t_{UO}|$).

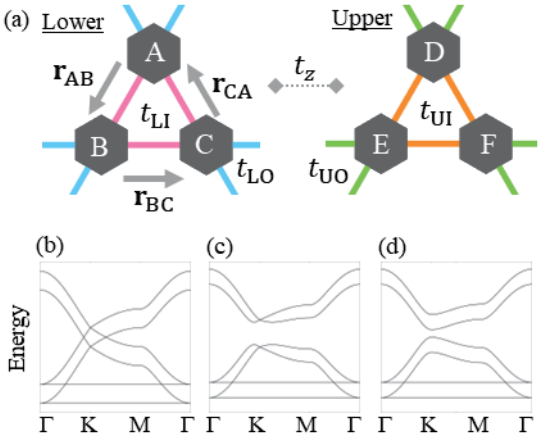

Fig. 1 (a) Schematic figure of bilayer Kagome lattice. Strengths of bonds (t_{LI}, t_{LO}, t_{UI}, t_{UO}) determines topological states. (b) Dispersion relation in N state, (c) L_+ and L_- states, and (d) V_+ and V_- states.

Dispersion relations of bilayer Kagome PnCs with various states are shown in **Fig. 1(b-d)**. Energy is doubly degenerated at K point and around K point in N state because of the symmetry protecting. If the symmetry is broken, *i.e.,* strengths of bonds are changed, degeneracy is lifted up and bandgap opens. By remaining some symmetry, $L_\pm$ states still have degenerate at K point.

3. Boundary mode with various types of edge shapes

There are three types of edge shapes in Kagome lattice. In this study, we focus on a straight boundary (**Fig. 2(a)**). We investigate topological boundary

E-mail: ‡y_hata@s.okayama-u.ac.jp, *tsuruta@okayama-u.ac.jp

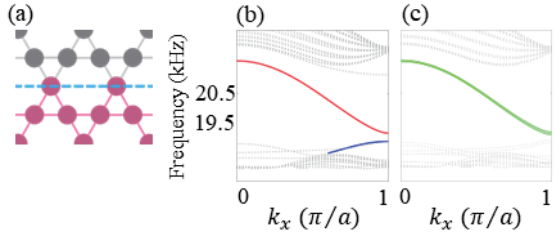

Fig. 2 (a) Straight boundary. (b) Dispersion relation of supercell with L_+ and L_- region. Red and blue lines denote polarized boundary modes in upper and lower layer. (c) Dispersion relation of supercell with V_+ and V_- region. Green lines show non-polarized boundary modes. In (b) and (c), gray dots show bulk and trivial boundary modes.

modes at straight edge shape with finite element method (FEM) simulations. We name each region by widths of bonds $(w_{LI}, w_{LO}, w_{UI}, w_{UO})$[mm] ; L_+: (1.5, 0.5, 0.5, 1.5), L_-: (0.5, 1.5, 1.5, 0.5), V_+: (0.5, 1.5, 0.5, 1.5), and V_-: (1.5, 0.5, 1.5, 0.5).

The dispersion relations and boundary modes are shown in **Fib. 2(b, c)**. There are polarized modes in upper layer from the top of bulk bands and lower layer from the bottom of bulk bands at a straight boundary between L_+ and L_- region (Fig. 2(b)). Group velocity of each mode has opposite sign. On the other hand, there are non-polarized modes from the top of bulk bands at a straight boundary between V_+ and V_- region (Fig. 2(c)). Group velocity of each mode has same sign, and these frequencies are almost the same as polarized modes in upper layer between L_+ and L_- region (Fig. 2(b)). Slight difference of these frequencies can be attributed to the symmetry breaking. In Fig. 2(b), polarized modes in upper and lower layer are inverted if the positions (red and gray region in Fig. 2(a)) of L_+ and L_- region are inverted. This is a natural consequence considering that the operation of inversion of region is equivalent to rotate 180° along boundary axis.

4. Multichannel waveguides

In this section, we design a multichannel waveguide using topological boundary modes demonstrated in previous section. Here the FEM simulations are conducted in frequency domain.

Displacement field of a layer converter is shown in **Fig. 3**. L_+/L_- regions are in left and right side and front-back position of L_+ and L_- is opposite. V_+/V_- region is in middle side. Pressure of 1Pa at 19.5 kHz along x direction is applied to a straight boundary of left side of the upper layer. First, the wave propagated in upper layer at left side, following with dispersion relation of Fig. 2(b). Second, both layers vibrated at middle side, following with Fig. 2(c). Finally, path of elastic wave changed to lower layer at right side because front-back position of L_+ and L_- region was opposite to left side.

5. Conclusion

We proposed bilayer Kagome PnCs which have layer DOF and investigate topological boundary modes with a straight edge shape. It is revealed that there are polarized modes in upper and lower layer at a boundary between L_+ and L_- region. In contrast, there is no polarized modes at a boundary between V_+ and V_- region. Finally, we demonstrated a multichannel waveguide which converts wave from one layer to another layer by FEM simulations. The present study paves the way to design multifunctional 3-dimensional elastic devices.

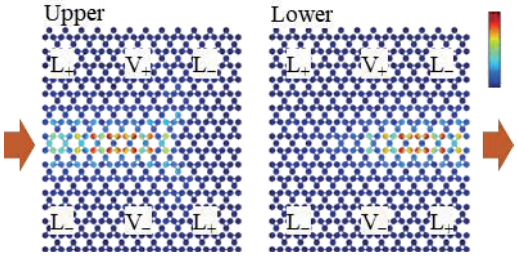

Fig. 3 Displacement filed of an elastic layer converter with a bilayer Kagome PnC. Input and output area show with arrows.

Acknowledgment

This work was supported by Japan Society for the Promotion of Science grant number JP21H05020.

References

1) Y. Hata, M. Misawa, and K. Tsuruta, 2023 IEEE Int. Ultrason. Symp., 2023, 1334 (Accepted).
2) X. Qi and S. Zhang, Rev. Mod. Phys. **83**, 1057 (2011).
3) K. Okuno and K. Tsuruta, Jpn. J. Appl. Phys. **59**, SKKA05 (2020).
4) H. Takeshita, M. Misawa, and K. Tsuruta, Proc. 42nd Symp. Ultrasonic Electronics, 2021, 3Pb1-2.
5) M. Kataoka, Y. Ohashi, M. Misawa, and K. Tsuruta, Proc. 43rd Symp. Ultrasonic Electronics, 2022, 3Pb1-1.
6) M. S. Ali, M. Kataoka, M. Misawa, and K. Tsuruta, Jpn. J. Appl. Phys. **62**, SJ1002 (2023).
7) M. Kataoka, M. Misawa, and K. Tsuruta, Symmetry 2022, **14**, 2133 (2022).
8) J. Lu, C. Qiu, W. Deng, X. Huang, F. Li, F. Zhang, S. Chen, and Z. Liu, Phys. Rev. Lett. **120**, 116802 (2018).
9) H. Li, Z. Wang, Z. Wang, C. Deng, J. Luo, J. Huang, X. Wang, and H. Yang, Appl. Phys. Lett. **121**, 243101 (2022).
10) Z. Wang, S. Liu, P. Yuan, and X. Xu, Appl. Phys. Lett. **120,** 191702 (2022).
11) M. Ezawa, Phys. Rev. Lett. **120**, 026801 (2018).
12) Q. Wu, H. Chen, X. Li, and G. Huang, Phys. Rev. Applied **14**, 014084 (2020).